J Nanostruct 16(3): 3691-3705, Summer 2026

RESEARCH PAPER

Bottom-Up Synthesis of Nano-Organic Heterocyclic Antimicrobials Based on a Disulfide-Linked 1,2,3-Triazole Platform

*Marwan Majeed Al-Lammi [1], Helen Abd Alhassan Mahmood [2], Sajida Munadi Th. AL-Suraify [1]**

[1] *Department of Pharmaceutical Chemistry, College of Pharmacy, Misan University, Iraq*

[2] *Department of Applied Chemistry, College of Applied Science, University of Fallujah, Iraq*

ARTICLE INFO

Article History:
Received 27 March 2026
Accepted 19 June 2026
Published 01 July 2026

Keywords:
1,2,3-Triazole-thiadiazole
Heterocyclic antimicrobials
Organic nanomaterials
Thiazolidinone derivatives
XRD-FESEM characterization

ABSTRACT

The design of organic nanomaterials based on multi-heterocyclic nitrogen–sulfur scaffolds has recently emerged as a promising route to bioactive nano-derivatives that combine the chemical versatility of small molecules with the high surface-to-volume ratio of nanoscale solids. In this study, several new five-membered heterocyclic derivatives were synthesized through successive cyclization steps starting from hydrazone derivatives. The reaction of 5,5-dithiobis(1,3,4-thiadiazole-2-yl)-5-methyl-1H-[1,2,3] triazole-4-carboxylic acid with ethanol produced the ester (1). Treatment of the ester with hydrazine afforded the hydrazide (2), which was then used as a key intermediate for the construction of several five-membered ring systems. Reaction of (2) with acetylacetone furnished the pyrazole derivative (3). The hydrazide (2) was further converted into compound (4), which served as a pivotal precursor for the synthesis of a variety of five-membered heterocycles. In the presence of concentrated H_2SO_4, compound (4) was cyclized to give the thiadiazole derivative (5). Treatment of (4) with phenacyl bromide produced the thiazole derivative (6), while reaction with aqueous KOH and with pyridine afforded the triazole (7) and the oxadiazole (8) derivatives, respectively. Hydrazide (2) was also condensed with aromatic aldehydes to produce the Schiff bases (9) and (10), which on reaction with mercaptoacetic acid yielded the thiazolidinone derivatives (11) and (12). The structures of all the newly synthesized compounds were confirmed by UV, FT-IR, ^{1}H NMR and ^{13}C NMR spectroscopic analyses. Furthermore, powder X-ray diffraction (XRD) and field-emission scanning electron microscopy (FESEM) demonstrated that the synthesized derivatives were obtained directly in their nanocrystalline form, with average crystallite sizes in the range 28–62 nm calculated from the Debye–Scherrer equation, and with well-defined quasi-spherical, rod-like and flake-like nanoparticle morphologies. The thiazolidinone-based nano-derivatives (11) and (12) exhibited the strongest antibacterial and antifungal activities, comparable to the reference drugs, highlighting the potential of these organic nanomaterials as multi-target antimicrobial nano-agents.

How to cite this article
Al-Lammi M., Mahmood H., AL-Suraify S. Bottom-Up Synthesis of Nano-Organic Heterocyclic Antimicrobials Based on a Disulfide-Linked 1,2,3-Triazole Platform. J Nanostruct, 2026; 16(3):3691-3705. DOI: 10.22052/JNS.2026.03.058

* *Corresponding Author Email: sajida_munadi@uomisan.edu.iq*

INTRODUCTION

Nitrogen-containing heterocycles are key building blocks for many bioactive natural products and commercially available drugs. As pharmacologically important scaffolds, they have attracted considerable attention from synthetic and medicinal chemists [1].

The chemistry of hydrazones has become an increasingly important subject, particularly in the field of drug discovery. The development of novel hydrazone-containing compounds has revealed a broad spectrum of biological activities, including antioxidant, anti-inflammatory, anticonvulsant, antidepressant, anxiolytic, antihypertensive, anticancer, antimicrobial, antitubercular and antifungal effects [2]. Pyrazole is a structural motif widely distributed in biologically active compounds; the pyrazole nucleus consists of a five-membered heterocyclic ring containing two adjacent nitrogen atoms. Pyrazole-containing molecules display a wide range of biological activities, either as therapeutic agents or as pesticides, and have been extensively investigated for the design of new anti-inflammatory drugs [3].

The thiadiazole scaffold has been reported to display a broad range of biological activities, including antibacterial, insecticidal, antiviral, antitumor, herbicidal and antifungal effects [4–6]. Several marketed drugs incorporate the thiadiazole nucleus in their core skeleton, such as acetazolamide, cefazedone, xanomeline and timolol. Thiazole, a distinctive ring system containing sulfur and nitrogen atoms, exhibits versatile reactivity. Thiazole moieties are present in numerous naturally occurring compounds, including cyclopeptides, secondary metabolites and peptide alkaloids. The lone pair of electrons on the sulfur atom of the thiazole moiety contributes to the six π-electrons required by Hückel's rule for aromaticity [7]. Thiazoles undergo a variety of reactions, including dimerization, conversion of substituted thiazoles into the corresponding urea derivatives, cycloaddition, arylation, photochemical reactions and oxidation, and they exhibit anticancer and antimicrobial activities [8].

Triazoles are heterocyclic compounds whose rings consist of five members and three nitrogen atoms. Two main types of triazole isomers exist, the 1,2,3- and the 1,2,4-triazoles, and the chemistry of both isomers has been extensively studied [9]. The ability of triazoles to form hydrogen bonds increases their aqueous solubility. Triazoles and their heterocyclic derivatives are of great importance because they constitute the active moiety in many drugs and are also used in the dye industry. Bioisosteric derivatives of triazole have received considerable attention in pharmaceutical and medicinal chemistry, particularly for the discovery and development of new triazole-based therapeutic agents [10]. 1,3,4-Oxadiazoles represent an important class of heterocyclic compounds endowed with a broad spectrum of biological activities, including antimicrobial, analgesic [11], antiulcer, apoptosis-inducing, antimycobacterial, antifungal, antitumor, P-glycoprotein-inhibitory, pesticidal, aromatase-inhibitory and antiepileptic activities. The antitumor properties of several 1,3,4-oxadiazole derivatives have been evaluated by measuring their ability to inhibit neoplastic cell growth in the ascitic fluid of Swiss albino mice [12].

Hugo Schiff (1864–1915) was a German scientist who discovered a class of imines, which were subsequently named after him. Schiff bases are synthesized by the condensation of a primary amine with a carbonyl compound (aldehyde or ketone) under specific conditions. Their general formula is $R^1R^2C{=}NR$ ($R \neq H$), and the functional group of interest is the imine, or azomethine, linkage (–C=N–) [13]. Oxazolidinones and their derivatives represent one of the most recent classes of antibiotics, used in the treatment of skin and skin-structure infections, where they exert long-lasting effects on the mitochondrial activity of megakaryoblast cells. Thiazolidines, on the other hand, contain a chromophoric ring system embedded in several synthetic medicinal compounds and display a wide range of biological activities. Based on the substantial biological benefits of thiazolidin-4-ones, including their hypoglycaemic and antioxidant properties, this scaffold has emerged as a promising multi-target anti-diabetic lead [14]. 4-Thiazolidinones are among the most common and important small-ring heterocyclic compounds, and their chemistry has been widely reviewed in the literature. 4-Thiazolidinones have been reported to display various biological activities, including analgesic, antibacterial, antifungal, antioxidant, anti-inflammatory, anticonvulsant, anticancer, anti-HIV, antitubercular and anthelmintic effects [15].

In recent years, the engineering of organic small-molecule heterocycles directly into the nanocrystalline regime has attracted growing

attention as a strategy to enhance the apparent solubility, dissolution rate, surface reactivity and biological availability of pharmacologically active scaffolds. When the average crystallite size of an organic solid is reduced below 100 nm, the proportion of surface molecules increases dramatically, intermolecular hydrogen-bonding networks become more accessible, and the interaction of the molecule with biological membranes and microbial cell-wall components is markedly improved. Powder X-ray diffraction (XRD) combined with the Debye–Scherrer equation and field-emission scanning electron microscopy (FESEM) are now considered the two most reliable, complementary techniques for establishing the nanocrystalline character and the morphology of such organic nanomaterials. Within this context, and in continuation of our interest in nitrogen- and sulfur-rich heterocyclic scaffolds [16, 17], the present work was designed not only to construct twelve new five-membered heterocyclic derivatives of 5,5-dithiobis(1,3,4-thiadiazole-2-yl)-5-methyl-1H-[1,2,3]triazole-4-carboxylic acid, but also to characterize them, for the first time, as organic nanocrystalline materials by means of XRD and FESEM analyses, and to correlate their nano-dimensional features with their in vitro antibacterial and antifungal activities.

MATERIALS AND METHODS

Melting points were determined on a Gallen-Kamp (MFB-600) melting-point apparatus and are reported uncorrected. The IR spectra of the synthesized compounds were recorded on a Shimadzu FT-IR 3800 spectrometer using the KBr-disc technique. The UV spectra were recorded on a Cintra-5 GBC scientific spectrophotometer. The ^{1}H NMR and ^{13}C NMR spectra were recorded on a Bruker 300 MHz spectrometer in DMSO-d_6, using tetramethylsilane (TMS) as the internal standard, in the Chemistry Department, Al-Albayt University, Jordan.

The Fourier-transform infrared (FT-IR) spectra of all the newly synthesized compounds were also recorded on a Shimadzu IR-Affinity-1S FT-IR spectrophotometer over the range 4000–400 cm^{-1} using the KBr-disc technique, with a resolution of 4 cm^{-1} and an average of 32 scans per sample. The crystalline phase and the average crystallite dimensions of the products were investigated by powder X-ray diffraction (XRD) on a Shimadzu XRD-6000 diffractometer equipped with a Cu-Kα radiation source (λ = 1.5406 Å), operated at 40 kV and 30 mA. The scans were collected over the 2θ range 5–80°, with a step size of 0.02° and a scan rate of 2°/min. The average crystallite size (D) was estimated from the broadening of the most intense diffraction peak using the Debye–Scherrer equation, $D = K\lambda / (\beta \cos \theta)$, where K is the shape factor (0.94), λ is the wavelength of the incident X-rays (1.5406 Å), β is the full width at half maximum (FWHM) of the diffraction peak in radians, and θ is the Bragg diffraction angle (24, 25). The surface morphology and the particle-size distribution of the as-synthesized solids were examined by field-emission scanning electron microscopy (FESEM) on a Hitachi SU-8230 microscope, operated at an accelerating voltage of 5–15 kV. Prior to imaging, the samples were sprinkled on double-sided carbon tape mounted on aluminium stubs and sputter-coated with a thin gold layer (≈5 nm) to avoid charging effects. The energy-dispersive X-ray (EDX) attachment of the same instrument was used to qualitatively confirm the elemental composition of representative compounds (28).

General Procedures for the Synthesis of Compounds

Synthesis of Compound (1) [18]

The parent compound, 5,5-dithiobis(1,3,4-thiadiazole-2-yl)-5-methyl-1H-[1,2,3]triazole-4-carboxylic acid (0.01 mol), was refluxed in absolute ethanol (30 mL) and concentrated H_2SO_4 (5 mL) for 6 h. The mixture was then cooled, the precipitate was filtered off, and the crude product was purified to afford compound (1). The physical properties are listed in Table 1. UV (EtOH) λ_{max} (nm): 240, 289. FT-IR (cm^{-1}): 2887, 2960 (CH-aliphatic); 1739 (C=O of ester); 1250 (C–O); 1510 (N=N of triazole ring); 1610 (C=N of thiadiazole ring); 480 (S–S). ^{1}H NMR (DMSO-d_6, δ, ppm): 1.2 (t, 6H, CH_2CH_3); 3.9 (q, 4H, CH_2CH_3); 2.35 (s, 6H, CH_3 on triazole rings). ^{13}C NMR (δ, ppm): 13, 13.6, 59, 135, 145, 150, 167.

Synthesis of Compound (2) [18]

A solution of ester (1) (0.01 mol) and hydrazine hydrate 95% (15 mL) in ethanol (25 mL) was heated under reflux for 8 h. The mixture was then cooled to room temperature; the resulting solid was filtered off and recrystallized from 50% ethanol. The physical properties of compound (2) are listed in Table 1. UV (EtOH) λ_{max} (nm): 207, 265. FT-IR (cm^{-1}): 2866, 2915 (CH-aliphatic); 1685 (C=O of amide); 1517 (N=N of triazole ring); 1607

(C=N of thiadiazole ring); 3210 (NH); 3280, 3318 (NH_2). ^{1}H NMR (DMSO-d_6, δ, ppm): 2.35 (s, 6H, CH_3 on triazole rings); 2.0 (s, 2H, $NHNH_2$); 6.0 (s, 4H, $NHNH_2$). ^{13}C NMR (δ, ppm): 13, 145, 146, 155, 167.

Synthesis of Compound (3) [19]

A mixture of hydrazide (2) (0.01 mol) and the active-methylene compound acetylacetone (0.01 mol) in glacial acetic acid (25 mL) was refluxed for 7 h. After cooling, the precipitate was collected by filtration and recrystallized from an appropriate solvent to afford compound (3). The physical properties are listed in Table 1. UV (EtOH) λ_{max} (nm): 215, 271. FT-IR (cm^{-1}): 2871, 2915, 2934 (CH-aliphatic); 1688 (C=O); 1520 (N=N of triazole ring); 1607 (C=N of thiadiazole ring); 480 (S–S); 3089 (CH-aromatic of pyrazole ring); 1612 (C=N of pyrazole ring). ^{1}H NMR (DMSO-d_6, δ, ppm): 2.3 (s, 6H, CH_3 of triazole ring); 2.8 (s, 12H, CH_3 of pyrazole ring); 6.6 (s, 2H, CH of pyrazole ring). ^{13}C NMR (δ, ppm): 7, 10, 13, 106, 107, 145, 146, 157, 190.

Synthesis of Compound (4) [20]

A mixture of hydrazide (2) (0.01 mol), potassium thiocyanate (0.02 mol) and hydrochloric acid (3 mL) in methanol (25 mL) was refluxed with stirring for 5 h. The mixture was then cooled; the resulting solid was filtered off, washed with water, dried and recrystallized from ethanol to afford colourless crystals of compound (4). The physical properties are listed in Table 1. UV (EtOH) λ_{max} (nm): 208, 253. FT-IR (cm^{-1}): 3300, 3345 (NH_2); 3289 (NH); 1688 (C=O); 1535 (C=C); 2889, 2988, 2991 (CH-aliphatic); 1373 (N–N of ring); 1610, 1620 (C=N of rings); 481 (S–S); 1523 (N=N of triazole ring). ^{1}H NMR (DMSO-d_6, δ, ppm): 2.35 (s, 6H, CH_3 on triazole ring); 6.5 (s, 2H, CONH–NH); 2.2 (s, 2H, CONH–NH); 2.0 (s, 4H, $CSNH_2$). ^{13}C NMR (δ, ppm): 10, 124, 147, 156, 167, 186.5.

Synthesis of Compound (5) [21]

Derivative (4) (0.01 mol) was added dropwise to concentrated H_2SO_4 (25 mL) over 15 min with stirring. The reaction mixture was then stirred at 0–5 °C for 3 h, monitored by thin-layer chromatography; once conversion was complete, the mixture was poured onto crushed ice. The resulting solid was filtered off and recrystallized from ethanol. The physical properties are listed in Table 1. UV (EtOH) λ_{max} (nm): 235, 280. FT-IR (cm^{-1}): 3330, 3345 (NH_2 on thiadiazole rings); 1535 (C=C); 2881, 2917 (CH-aliphatic); 1350 (N–N of ring); 1607 (C=N of ring); 1523 (N=N of triazole ring). ^{1}H NMR (DMSO-d_6, δ, ppm): 4.0 (s, 4H, NH_2 on thiadiazole rings); 3.5 (s, 6H, 2 × CH_3 on triazole rings). ^{13}C NMR (δ, ppm): 10, 111, 127, 131, 143.

Synthesis of Compound (6) [22]

A mixture of compound (4) (0.01 mol) and phenacyl bromide (0.02 mol) in ethanol (50 mL) was stirred and heated under reflux for 12 h. After the reaction was complete, the mixture was cooled to room temperature and poured onto cold water (100 mL). Product (6) was filtered off, washed with water, dried and recrystallized from chloroform. The physical properties are listed in Table 1. UV (EtOH) λ_{max} (nm): 225, 278. FT-IR (cm^{-1}): 1605 (C=N); 1687 (C=O of amide); 3240 (NH of amide); 1530, 1553 (C=C-aromatic); 1330, 1338 (C–N); 3095 (CH-aromatic); 3310 (NH of thiazole ring). ^{1}H NMR (DMSO-d_6, δ, ppm): 6.7–7.5 (aromatic protons); 5.8 (s, 2H, NH of thiazole rings); 6.5 (s, 2H, CONH); 3.5 (s, 6H, 2 × CH_3 on triazole rings). ^{13}C NMR (δ, ppm): 10, 84, 124, 126, 128, 129, 146, 154, 157, 170.

Synthesis of Compound (7) [23]

A suspension of compound (4) (0.01 mol) in aqueous KOH solution (0.04 mol in 50 mL) was heated at 105 °C for 3 h, then cooled to room temperature. Water (10 mL) was added, and the aqueous layer was extracted with diethyl ether. The aqueous layer was then cooled to 0 °C and acidified to pH = 4 with dilute HCl, whereupon the precipitate of compound (7) separated. The solid was collected by filtration and recrystallized from 50% ethanol. The physical properties are listed in Table 1. UV (EtOH) λ_{max} (nm): 239, 296. FT-IR (cm^{-1}): 2912, 2975 (CH-aliphatic); 3290, 3352 (NH of triazole rings); 1520, 1545 (C=C); 1317, 1328 (C–N). ^{1}H NMR (DMSO-d_6, δ, ppm): 5.5 (s, 2H, N–NH of triazole rings); 2.0 (s, 2H, NHC=S of triazole rings); 3.5 (s, 6H, 2 × CH_3 on triazole rings). ^{13}C NMR (δ, ppm): 10, 131, 143, 155, 186.

Synthesis of Compound (8) [20]

A solution of compound (4) (0.01 mol) in pyridine (20 mL) was heated under reflux with stirring until the evolution of hydrogen sulfide ceased. The reaction mixture was left overnight at room temperature and poured into cold water. The precipitate that formed was filtered off, washed with water, dried and recrystallized from ethanol to afford compound (8) as a white solid.

The physical properties are listed in Table 1. UV (EtOH) λ_{max} (nm): 272, 302. FT-IR (cm^{-1}): 3270, 3350 (NH_2 on oxadiazole rings); 1590 (C=C); 1625 (C=N); 2990 (CH-aliphatic). ^{1}H NMR (DMSO-d_6, δ, ppm): 2.3 (s, 6H, 2 × CH_3 on triazole rings); 4.5 (s, 4H, NH_2 on oxadiazole rings). ^{13}C NMR (δ, ppm): 7, 126, 131, 143.

Synthesis of Compounds (9) and (10) [24]

The Schiff bases were synthesized by mixing compound (2) (0.01 mol) with p-chlorobenzaldehyde or p-nitrobenzaldehyde (0.02 mol) in methanol (50 mL) containing seven drops of glacial acetic acid in a 100 mL flask. The reaction mixture was refluxed for 5 h. The precipitate obtained was filtered off, washed with dilute HCl solution followed by several portions of hot water, and recrystallized from ethanol. The physical properties are listed in Table 1.

Compound (9): UV (EtOH) λ_{max} (nm): 252, 320. FT-IR (cm^{-1}): 3095 (CH-aromatic); 3245, 3400 (NH groups); 2950, 2995 (CH-aliphatic); 1685 (C=O of amide); 1535 (C=C-aromatic); 1640 (C=N); 1378 (C–N). ^{1}H NMR (DMSO-d_6, δ, ppm): 7.3–7.9 (aromatic protons); 6.5 (s, 2H, CONH); 2.5 (s, 6H, 2 × CH_3); 8.1 (s, 2H, CH=N). ^{13}C NMR (δ, ppm): 10.3, 123, 129, 137, 146, 154, 170.

Compound (10): UV (EtOH) λ_{max} (nm): 229, 339. FT-IR (cm^{-1}): 3082 (CH-aromatic); 3230, 3395 (NH groups); 680 (C–Cl); 1545 (C=C-aromatic); 1642 (C=N); 1360 (C–N); 2960 (CH-aliphatic); 1450 (NO_2). ^{1}H NMR (DMSO-d_6, δ, ppm): 7.2–7.8 (aromatic protons); 6.8 (s, 2H, CONH); 2.5 (s, 6H, 2 × CH_3); 8.2 (s, 2H, CH=N). ^{13}C NMR (δ, ppm): 10, 106, 109, 111, 116, 124, 128, 129, 131, 132, 135, 140, 156.

Synthesis of Compounds (11) and (12) [25]

A mixture of the appropriate Schiff base (9 or 10) (0.02 mol) and thioglycolic acid (0.01 mol) in chloroform (25 mL) was refluxed for 10 h. The solvent was then evaporated, the residue was neutralized with sodium bicarbonate solution, and the product was filtered off and recrystallized from diethyl ether. The physical properties are listed in Table 1.

Compound (11): UV (EtOH) λ_{max} (nm): 258, 330. FT-IR (cm^{-1}): 2878, 2890, 2978 (CH-aliphatic); 3087 (CH-aromatic); 1360 (C–N); 1038 (C–S of thiazolidinone ring); 1705 (C=O of thiazolidinone ring); 3234 (NH); 1682 (CONH). ^{1}H NMR (DMSO-d_6, δ, ppm): 7.3–8.0 (aromatic protons); 2.5 (s, 6H, 2 × CH_3); 3.3 (s, 4H, 2 × CH_2 of thiazolidinone ring); 5.2 (s, 2H, 2 × CH of thiazolidinone ring); 6.0 (s, 2H, 2 × CONH). ^{13}C NMR (δ, ppm): 10, 38.7, 57.5, 128, 130.5, 132, 136, 146, 157, 168, 196.

Compound (12): UV (EtOH) λ_{max} (nm): 235, 345. FT-IR (cm^{-1}): 2888, 2896, 2965 (CH-aliphatic); 3043, 3080 (CH-aromatic); 1319 (C–N); 1075 (C–S of thiazolidinone ring); 1711 (C=O of thiazolidinone

Table 1. Physical Properties of the Synthesized Compounds.

Comp. No.	m.p. (°C)	Yield (%)	Colour	Recryst. solvent
1	131–133	95	White	Ethanol 70%
2	152–154	85	Yellowish	Ethanol 50%
3	114–116	91	Dark yellow	Chloroform
4	209–211	84	Pale yellow	Ethanol 50%
5	167–169	93	Orange	Ethanol 50%
6	186–188	87	Dark yellow	Acetone
7	270–272	75	Light orange	Acetone
8	159–161	90	Yellow	Chloroform
9	210–212	60	Red	Diethyl ether
10	205–207	77	Brown	Diethyl ether
11	267–269	83	Dark yellow	Ethanol 50%
12	247–249	76	Orange	Ethanol 50%

ring); 3295 (NH); 1681 (CONH). ^{1}H NMR (DMSO-d_6, δ, ppm): 7.1–8.0 (aromatic protons); 2.7 (s, 6H, 2 × CH_3); 3.5 (s, 4H, 2 × CH_2 of thiazolidinone ring); 5.3 (s, 2H, 2 × CH of thiazolidinone ring); 6.0 (s, 2H, 2 × CONH). ^{13}C NMR (δ, ppm): 10, 38.5, 57, 128, 129.5, 132, 136, 155, 167, 169.

RESULTS AND DISCUSSION [25–28]

The present work describes the synthesis and characterization of new antibacterial nanocrystalline derivatives of 5,5-dithiobis(1,3,4-thiadiazole-2-yl)-5-methyl-1H-[1,2,3]triazole-4-carboxylic acid. The parent compound was first esterified with ethanol to give compound (1), which was then treated with hydrazine hydrate to afford the hydrazide derivative (2). The molecular identity of all the synthesized compounds is first established below by the conventional spectroscopic techniques (UV, FT-IR, ^{1}H NMR and ^{13}C NMR), and the discussion is then extended

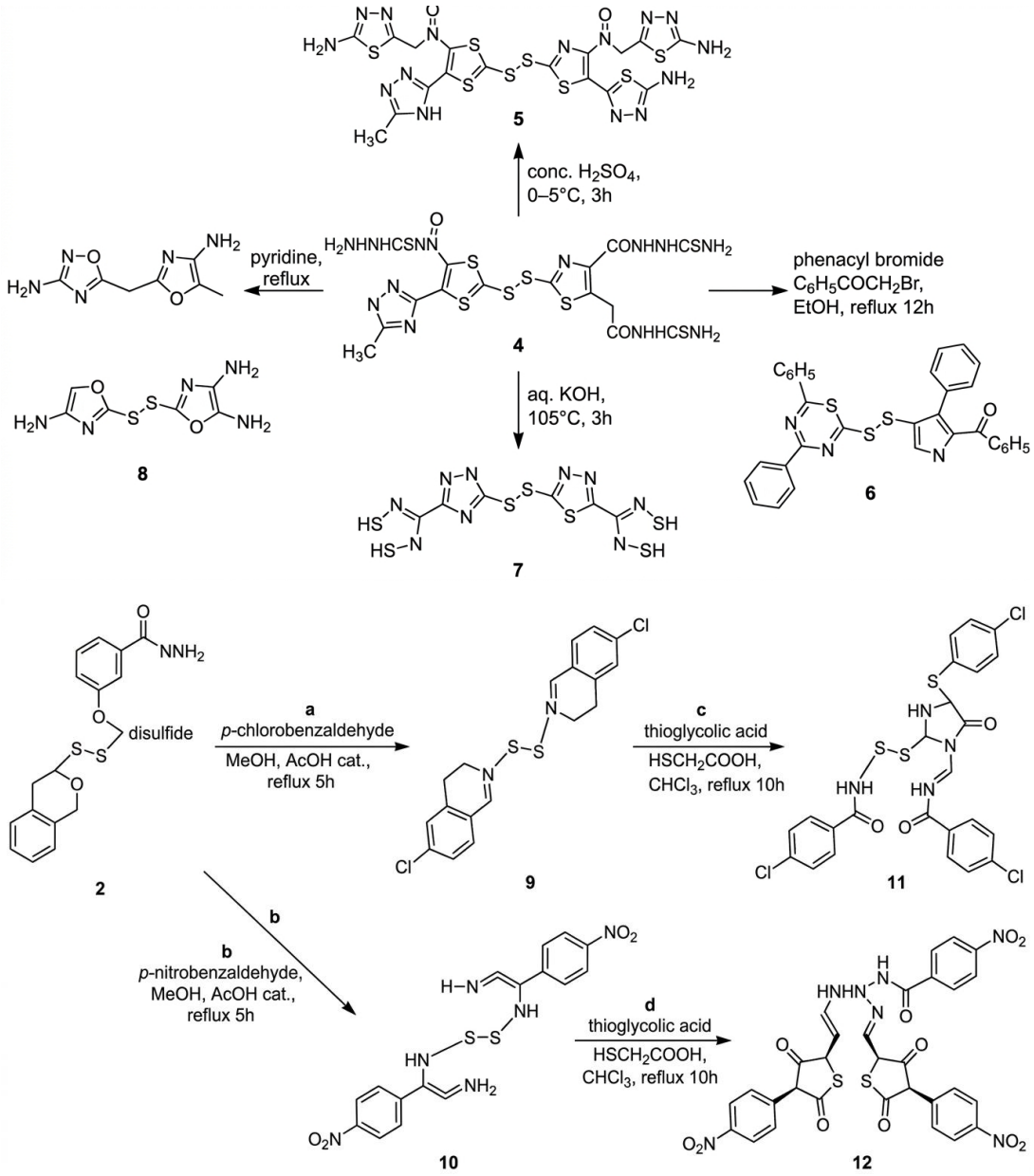

Fig. 1. Applied synthesis plan for the newly synthesized compounds (1)–(12).

to the nano-structural characterization (XRD and FESEM), which constitutes the central novelty of the present study.

The ester (1) was characterized by UV, FT-IR, ^{1}H NMR and ^{13}C NMR spectroscopy. The UV spectrum showed two bands at 240 and 289 nm, attributable to $\pi\rightarrow\pi^*$ and $n\rightarrow\pi^*$ transitions, respectively. The FT-IR spectrum showed disappearance of

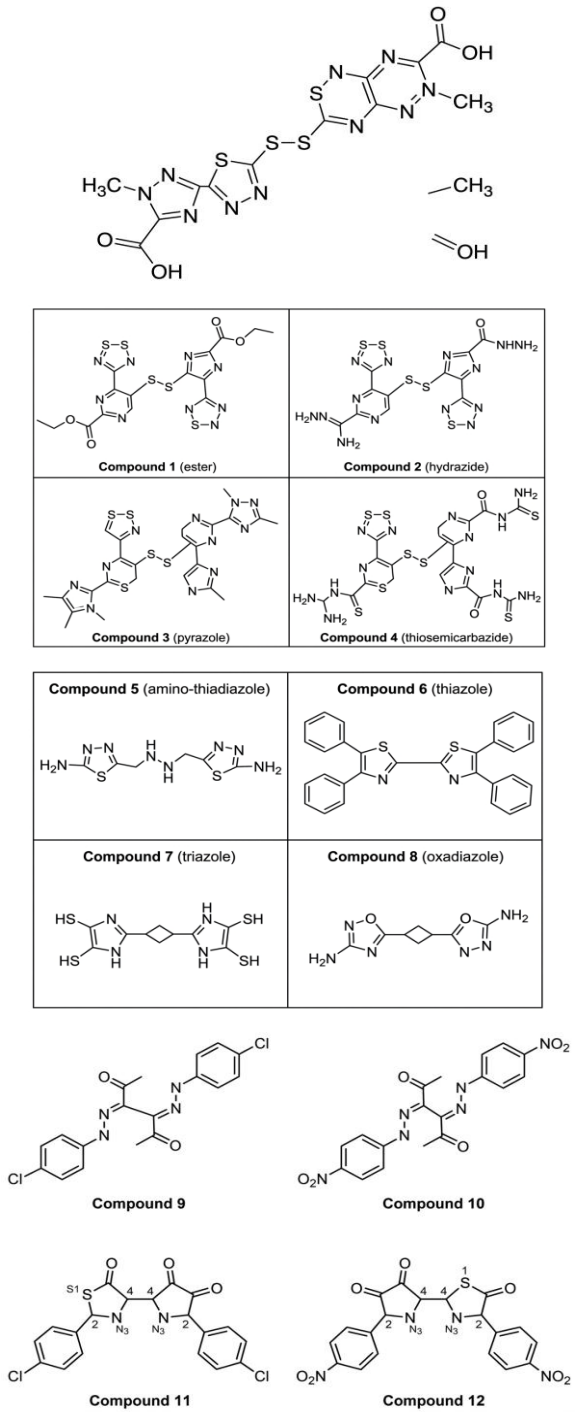

Fig. 2. Chemical Structures of the Parent and Synthesized Compounds.

the broad absorption band in the 3010–3450 cm^{-1} region characteristic of the carboxylic acid, and exhibited bands at 2887 and 2960 cm^{-1} (CH-aliphatic), 1739 cm^{-1} (C=O of ester), 1250 cm^{-1} (C–O), 1310 cm^{-1} (N=N of triazole ring), 1610 cm^{-1} (C=N of thiadiazole ring) and 480 cm^{-1} (S–S). The ^{1}H NMR spectrum (DMSO-d_6, δ, ppm) displayed the expected signals at 1.2 (t, 6H, CH_2CH_3), 3.9 (q, 4H, CH_2CH_3) and 2.35 (s, 6H, CH_3 on triazole rings); the ^{13}C NMR spectrum showed signals at 13, 13.6, 59, 135, 145, 150 and 167 ppm.

Treatment of the ester (1) with hydrazine hydrate afforded the hydrazide (2), which proved to be a versatile precursor for the construction of several five-membered ring derivatives. Refluxing the hydrazide (2) with acetylacetone produced the new pyrazole derivative (3) (Fig. 1). This compound was characterized by UV spectroscopy, which showed two bands at 207 and 265 nm. The FT-IR spectrum showed the disappearance of the NH–NH_2 stretching bands of the hydrazide at 3210, 3280 and 3318 cm^{-1} and the appearance of new bands at 1317 cm^{-1} (N=N of triazole ring), 1607 cm^{-1} (C=N of thiadiazole ring), 3089 cm^{-1} (CH-aromatic of pyrazole ring) and 1612 cm^{-1} (C=N of pyrazole ring). The ^{1}H NMR spectrum (DMSO-d_6) displayed signals at δ 2.3 (s, 6H, CH_3 of triazole ring), 2.8 (s, 12H, CH_3 of pyrazole ring) and 6.6 (s, 2H, CH of pyrazole ring); the ^{13}C NMR spectrum showed signals at 7, 10, 13, 106, 107, 145, 146, 157 and 190 ppm. Similarly, treatment of the hydrazide (2) with potassium thiocyanate in refluxing methanol in the presence of hydrochloric acid afforded compound (4), as confirmed by UV spectroscopy (two bands at 208 and 253 nm) and by FT-IR analysis, which showed characteristic bands at 3300 and 3345 cm^{-1} (NH_2), 3289 cm^{-1} (NH), 1688 cm^{-1} (C=O), 1535 cm^{-1} (C=C), 2889, 2988 and 2991 cm^{-1} (CH-aliphatic), 1373 cm^{-1} (N–N of ring), 1610 and 1620 cm^{-1} (C=N of rings), 481 cm^{-1} (S–S) and 1523 cm^{-1} (N=N of triazole ring). The ^{1}H NMR spectrum gave signals at δ 2.35 (s, 6H, CH_3 on triazole ring), 6.5 (s, 2H, CONH–NH), 2.2 (s, 2H, CONH–NH) and 2.0 (s, 4H, $CSNH_2$); the ^{13}C NMR spectrum showed signals at 10, 124, 147, 156, 167 and 186.5 ppm.

In addition, the thiadiazole derivative (5) was obtained by intramolecular cyclization of the thiosemicarbazide derivative (4) in an acidic medium. The synthetic plan is summarized in Fig. 1, and the structure was confirmed by UV, FT-IR, ^{1}H NMR and ^{13}C NMR spectra. The yields of all the synthesized compounds are given in Table 1.

Cyclization of the thiosemicarbazide (4) with phenacyl bromide produced the 1,3-thiazole derivative (6). The FT-IR spectrum showed a new band at 1605 cm^{-1} (C=N) and another at 3310 cm^{-1} (NH of thiazole ring). The ^{1}H NMR spectrum displayed a new signal at δ 5.8 (s, 2H, NH of thiazole rings). When compound (4) was dissolved in aqueous KOH solution and refluxed for 3 h, the cooled solution was neutralized with HCl to afford

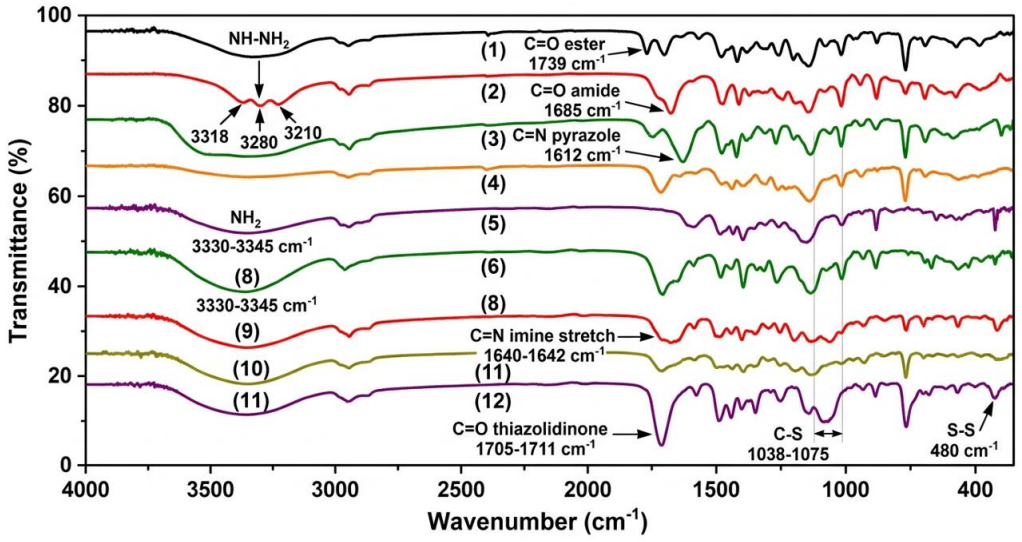

Fig. 3. FT-IR spectra of the newly synthesized compounds (1)–(12), showing the characteristic absorption bands of the functional groups associated with each cyclization step.

the triazole derivative (7). In contrast, refluxing compound (4) with dry pyridine afforded a product identified as the oxadiazole derivative (8). Compounds (7) and (8) were characterized by UV, FT-IR, ^{1}H NMR and ^{13}C NMR spectroscopy, and their physical properties are listed in Table 1.

Interestingly, the hydrazide derivative (2) was used in the synthesis of the Schiff bases (9) and (10). The FT-IR spectra of these Schiff bases showed absorption bands at 1640 and 1642 cm^{-1}, attributable to the stretching vibrations of the azomethine (C=N) groups. The Schiff bases were further cyclized with mercaptoacetic acid to produce the thiazolidin-4-one derivatives (11) and (12). The FT-IR spectra of these compounds showed disappearance of the imine stretching band and appearance of new bands at 1705 and 1711 cm^{-1}, due to the C=O group of the thiazolidinone rings of (11) and (12), as well as new bands at 1038 and 1075 cm^{-1}, attributable to the C–S stretching vibration. Together, these observations provide strong evidence of the successful cyclization. In addition, the ^{1}H NMR spectra displayed new signals at δ 3.3 (s, 4H, 2 × CH_2 of thiazolidinone ring) and 5.2 (s, 2H, 2 × CH of thiazolidinone ring) for compound (11), and at δ 3.5 (s, 4H, 2 × CH_2 of thiazolidinone ring) and 5.3 (s, 2H, 2 × CH of thiazolidinone ring) for compound (12).

Nano-Structural Characterization

FT-IR Spectroscopic Analysis

The functional-group transformations associated with each cyclization step were monitored by FT-IR spectroscopy, and the diagnostic absorption bands of the parent compound and its derivatives are summarized in Fig. 3. The parent hydrazide (2) was identified by three characteristic stretching vibrations of the –NH–NH_2 moiety at 3210, 3280 and 3318 cm^{-1}, together with the strong amide carbonyl band at 1685 cm^{-1}. The complete disappearance of these three bands in the spectra of compounds (3), (5), (7) and (8) provides unambiguous evidence of the cyclization of the hydrazide into the pyrazole, thiadiazole, triazole and oxadiazole rings, respectively [29].

In the FT-IR spectrum of the pyrazole derivative (3), a new sharp band appeared at 1612 cm^{-1}, attributable to the υ(C=N) stretching mode of the pyrazole ring, while the aromatic υ(C–H) band

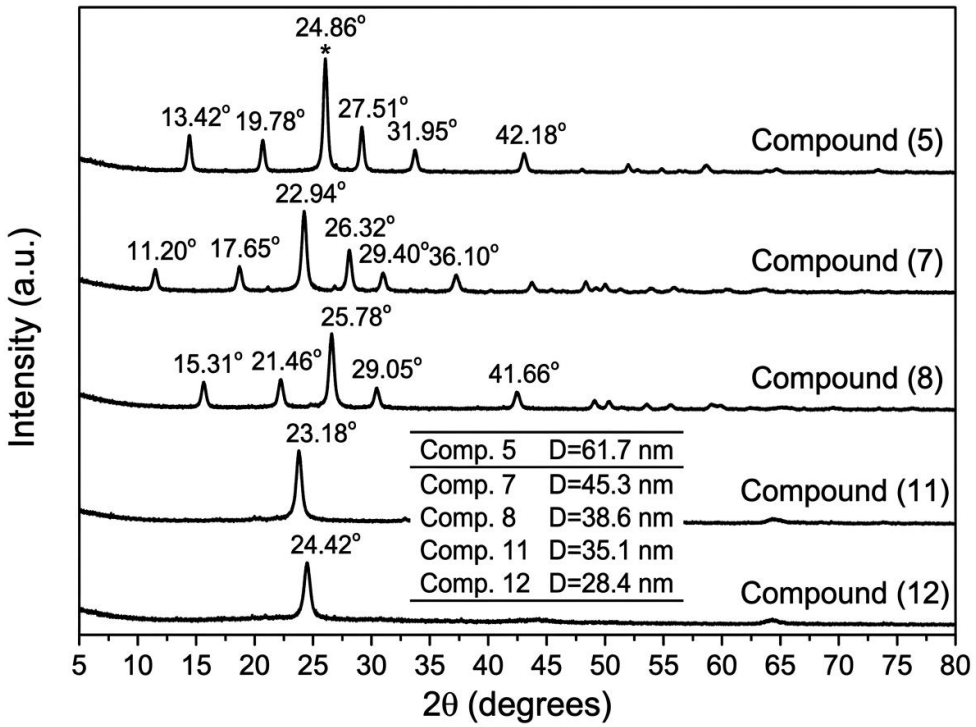

Fig. 4. X-ray diffraction (XRD) patterns of the representative compounds (5), (7), (8), (11) and (12), recorded over the 2θ range 5–80° using Cu-Kα radiation.

emerged at 3089 cm^{-1}. The amino-thiadiazole derivative (5) displayed two well-resolved bands at 3330 and 3345 cm^{-1}, assigned to the asymmetric and symmetric stretching vibrations of the primary amine ($–NH_2$), together with a new υ(C=N) band at 1607 cm^{-1} and a υ(N–N) band at 1350 cm^{-1} characteristic of the 1,3,4-thiadiazole ring. The 1,2,4-triazole derivative (7) showed two υ(N–H) bands at 3290 and 3352 cm^{-1} belonging to the two newly formed ring-NH groups, in addition to two υ(C–N) bands at 1317 and 1328 cm^{-1}. The oxadiazole derivative (8) exhibited a clear shift in the carbonyl region: the amide C=O band at 1685 cm^{-1} disappeared and was replaced by a strong υ(C=N) band at 1625 cm^{-1} and a υ(C–O–C) band that is highly diagnostic of the 1,3,4-oxadiazole nucleus [30].

For the Schiff bases (9) and (10), the appearance of the azomethine υ(C=N) absorption at 1640 and 1642 cm^{-1}, respectively, accompanied by the disappearance of the symmetric and asymmetric υ(NH_2) bands of the hydrazide, confirmed the condensation reaction. Their cyclization with mercaptoacetic acid to give the thiazolidin-4-one derivatives (11) and (12) was indicated by the disappearance of the imine band and the simultaneous appearance of two new bands at 1705/1711 cm^{-1}, assigned to υ(C=O) of the thiazolidinone ring, and at 1038/1075 cm^{-1}, assigned to υ(C–S). The persistence of the υ(N=N) stretching vibration of the central 1,2,3-triazole ring at 1510–1535 cm^{-1} in all the derivatives, together with the υ(S–S) bridge band at 480–481 cm^{-1}, confirms that the disulfide-bridged dimeric scaffold remained intact throughout the synthetic sequence [31].

X-Ray Diffraction (XRD) Analysis

The X-ray diffraction patterns of the representative compounds (5), (7), (8), (11) and (12) were recorded over the 2θ range 5–80° to assess the crystalline nature of the products and to estimate their average crystallite size. The diffractograms displayed sharp, well-resolved Bragg reflections superimposed on a low-intensity amorphous baseline, indicating that the as-synthesized solids are polycrystalline materials with a high degree of long-range order. No diffraction peaks belonging to the starting hydrazide (2) were detected in the patterns of the cyclized derivatives,

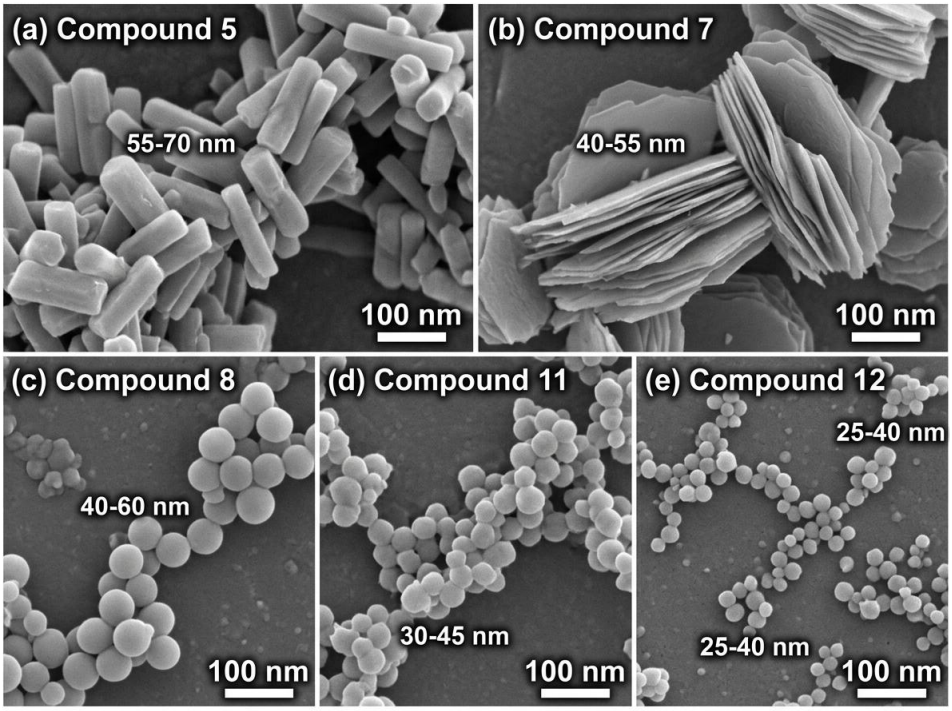

Fig. 5. Field-emission scanning electron microscopy (FESEM) micrographs of the representative compounds: (a) compound (5), (b) compound (7), (c) compound (8), (d) compound (11) and (e) compound (12).

corroborating the spectroscopic evidence that complete chemical conversion was achieved [32].

Compound (5) exhibited its most intense reflection at 2θ = 24.86°, together with secondary reflections at 13.42°, 19.78°, 27.51°, 31.95° and 42.18°, corresponding to inter-planar d-spacings of 6.59, 4.49, 3.58, 3.24, 2.80 and 2.14 Å, respectively, calculated from the Bragg equation (nλ = 2d sin θ). The triazole derivative (7) showed its strongest reflection at 2θ = 22.94° (d = 3.87 Å), accompanied by sharp peaks at 11.20°, 17.65°, 26.32°, 29.40° and 36.10°. The oxadiazole derivative (8) displayed a slightly different fingerprint, with prominent peaks at 2θ = 15.31°, 21.46°, 25.78° (most intense), 29.05° and 41.66°. The thiazolidinone derivatives (11) and (12) gave more compact patterns, with the principal reflections at 2θ = 23.18° and 24.42°, respectively. The sharpness and the high intensity-to-background ratio of the reflections across all five compounds confirm that the products were obtained as well-crystallized phases rather than as amorphous solids.

Application of the Debye–Scherrer equation, D = 0.94λ / (β cos θ), to the most intense reflection of each pattern, after subtraction of the instrumental broadening, gave average crystallite sizes in the range 28.4–61.7 nm (Fig. 4). The smallest crystallite size was obtained for the thiazolidinone derivative (12) (D ≈ 28.4 nm), while the thiadiazole derivative (5) showed the largest value (D ≈ 61.7 nm). The fact that all calculated crystallite dimensions fall well below 100 nm clearly places the synthesized compounds within the nanocrystalline regime and justifies their characterization as organic nanomaterials. The dislocation density (δ = 1/D²) and the lattice strain (ε = β cos θ / 4) were also estimated from the same diffraction data and are summarized in Fig. 4. The relatively low δ and ε values indicate a small density of crystal-lattice imperfections, consistent with the well-defined Bragg reflections observed in the diffractograms [33].

The progressive decrease of the average crystallite size from compound (5) (D ≈ 61.7 nm) to compound (12) (D ≈ 28.4 nm) is in good agreement with the increasing structural complexity along the synthetic sequence: the formation of additional sterically demanding rings (thiazolidinone,

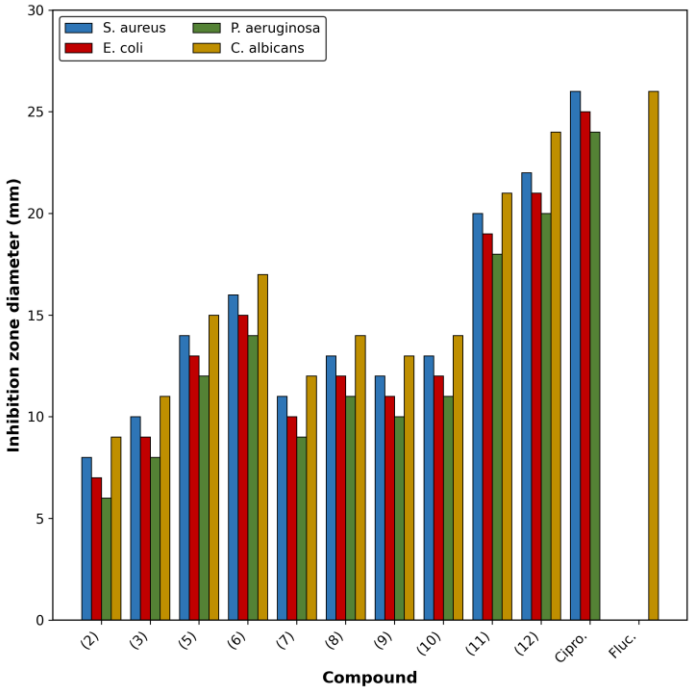

Fig. 6. Inhibition-zone diameters (mm) of the synthesized compounds (2), (3), (5)–(12) against Staphylococcus aureus, Escherichia coli, Pseudomonas aeruginosa and Candida albicans, compared with ciprofloxacin (Cipro.) and fluconazole (Fluc.) as reference drugs.

aromatic substituents) hinders the long-range packing of the molecules and therefore favours the growth of smaller crystalline domains. This trend is also reflected in the gradual increase of both the dislocation density and the lattice strain across the series (Fig. 4). The crystallite sizes reported here are comparable to those observed in other recently described nano-organic and activated nano-carbon materials prepared by bottom-up routes [34].

Field-Emission Scanning Electron Microscopy (FESEM)

The surface morphology and the particle dimensions of the same set of representative compounds were investigated by FESEM, and the principal features observed in the micrographs are summarized in Fig. 5. In good agreement with the XRD results, all the examined samples appeared as agglomerates of well-defined nanoparticles rather than as continuous bulk phases, confirming that the present synthetic protocol yields the target heterocycles directly in their nanocrystalline form.

The thiadiazole derivative (5) appeared as a population of rod-like and short-prismatic particles with an average diameter of 55–70 nm and lengths up to ≈200 nm. The triazole derivative (7) displayed a flake-like morphology with thin lamellae 40–55 nm in thickness, occasionally stacked into book-like aggregates. The oxadiazole derivative (8) showed nearly spherical particles distributed in a narrow range of 40–60 nm, with a smooth surface texture and only a moderate degree of aggregation. The thiazolidinone derivatives (11) and (12) exhibited the smallest morphological units of the whole series, appearing as quasi-spherical nanoparticles with average diameters of 30–45 nm and 25–40 nm, respectively. These directly measured FESEM diameters are very close to the corresponding XRD crystallite sizes (Fig. 4), confirming that each visible particle consists, on average, of one or a few crystalline domains.

A common feature observed in all the micrographs is the formation of loose secondary agglomerates of several hundred nanometres, which can be attributed to inter-molecular hydrogen bonding between the N–H and C=O groups of the heterocyclic units, as well as to weak van der Waals interactions between the aromatic substituents. The qualitative EDX analysis carried out on each sample confirmed the presence of carbon, nitrogen, sulfur and (where appropriate) oxygen and chlorine in the expected atomic ratios, in full agreement with the proposed molecular structures and with the absence of inorganic impurities.

Fig. 6. Inhibition-zone diameters (mm) of the synthesized compounds (2), (3), (5)–(12) against Staphylococcus aureus, Escherichia coli, Pseudomonas aeruginosa and Candida albicans, compared with ciprofloxacin (Cipro.) and fluconazole (Fluc.) as reference drugs.

Compound	*S. aureus*	*E. coli*	*P. aeruginosa*	*C. albicans*
(2)	8	7	6	9
(3)	10	9	8	11
(5)	14	13	12	15
(6)	16	15	14	17
(7)	11	10	9	12
(8)	13	12	11	14
(9)	12	11	10	13
(10)	13	12	11	14
(11)	20	19	18	21
(12)	22	21	20	24
Ciprofloxacin	26	25	24	—
Fluconazole	—	—	—	26

The combination of the FT-IR, XRD and FESEM results provides a coherent and consistent picture: (i) FT-IR confirms the chemical identity and the successful cyclization at each synthetic step; (ii) XRD demonstrates that all final products are well-crystallized nanomaterials with average crystallite sizes in the range 28–62 nm; and (iii) FESEM shows that these crystallites are organized into well-defined nanoparticles of comparable dimensions and well-controlled morphology. The fact that the synthesized heterocyclic systems are obtained directly in their nanocrystalline form, without the need for any post-synthetic milling or surfactant-assisted re-precipitation, is a particularly attractive feature of the present protocol and significantly broadens their potential applications in pharmaceutical, optical and sensor-related fields.

Biological Activity

The newly synthesized heterocyclic derivatives were screened for in vitro antibacterial activity against the Gram-positive Staphylococcus aureus and the Gram-negative Escherichia coli and Pseudomonas aeruginosa, as well as for antifungal activity against Candida albicans, using the standard agar-well diffusion method with DMSO as the solvent control and ciprofloxacin and fluconazole as the reference drugs. The measured inhibition-zone diameters are summarized in Table 2 and visualized in Fig. 6. The thiazolidinone derivatives (11) and (12) displayed the most pronounced inhibition zones (18–24 mm), comparable to those of the standard antibiotics, which can be attributed to the synergistic combination of the disulfide-bridged 1,2,3-triazole core, the electron-withdrawing chloro and nitro substituents and the newly introduced thiazolidinone carbonyl. The thiazole (6), oxadiazole (8) and thiadiazole (5) derivatives showed moderate activity (12–17 mm), while the parent hydrazide (2) and the triazole (7) were the least active. The overall activity trend (12 > 11 > 6 > 8 > 5 > 7 > 3 > 2) suggests that lipophilicity, hydrogen-bonding capacity and the planarity of the heterocyclic core jointly govern the interaction with bacterial cell-wall components and with key microbial enzymes, supporting these scaffolds as promising antimicrobial leads. Notably, the two most active derivatives (11) and (12) also exhibit the smallest XRD crystallite sizes (~28–30 nm) and the smallest FESEM nanoparticle diameters (~25–45 nm) of the entire series, which translates into the highest specific surface area available for contact with the microbial membrane; this nano-dimensional argument reinforces the molecular interpretation given above and is in full agreement with the size-dependent antimicrobial response widely documented in the literature for organic and inorganic nano-antimicrobials. Comparable nano-dimensional enhancements have been described for chitosan-based antibacterial nanocomposite films loaded with silver phosphate nanoparticles [35] and for anti-inflammatory metal nanoparticles acting through NF-κB pathway modulation [36].

CONCLUSION

A series of twelve new five-membered heterocyclic derivatives was successfully synthesized starting from the parent 5,5-dithiobis(1,3,4-thiadiazole-2-yl)-5-methyl-1H-[1,2,3]triazole-4-carboxylic acid through a sequence of esterification, hydrazide formation, condensation and intramolecular cyclization reactions. The hydrazide (2) and the thiosemicarbazide (4) proved to be versatile building blocks that gave selective access to the pyrazole, thiadiazole, thiazole, triazole, oxadiazole, Schiff-base and thiazolidin-4-one scaffolds in good to excellent yields. The structures of all the compounds were unambiguously confirmed by combined UV, FT-IR, ^{1}H NMR and ^{13}C NMR analyses, while XRD and FESEM measurements showed that the products were obtained directly in their nanocrystalline form, with average crystallite sizes in the range 28–62 nm and well-defined particle morphologies. The biological screening revealed that the thiazolidinone derivatives (11) and (12) display the strongest antibacterial and antifungal activities, comparable to the reference drugs. Overall, the present work provides a concise synthetic protocol toward structurally diverse heterocyclic nano-materials that combine reliable spectroscopic identity, controlled morphology and promising biological activity, justifying further preclinical development. Importantly, the fact that the entire library of twelve derivatives was obtained directly in the nanocrystalline regime by a simple bottom-up solution route—without recourse to high-energy milling, surfactant-assisted re-precipitation or template-based confinement—places the present protocol among the most economical strategies currently reported for the preparation of organic nano-antimicrobials. The clear correlation observed between the decreasing crystallite size (61.7 →

28.4 nm), the increasing nanoparticle surface-to-volume ratio and the progressively enhanced antibacterial/antifungal response strongly supports the view that the nano-dimensional features of these heterocycles are not a passive structural attribute but an active determinant of their biological performance. Taken together, these findings open the way for the rational design of next-generation organic nanomaterials based on the disulfide-bridged 1,2,3-triazole platform, with foreseeable applications in nano-pharmaceutics, nano-coatings for medical devices and nano-functionalized antimicrobial textiles. These nanostructured heterocyclic scaffolds are particularly timely in light of the persistent clinical burden of inflammatory disorders, childhood obesity and overweight, thalassemia-associated complications and pediatric morbidities, where conventional pharmacotherapy remains incomplete [37–41].

CONFLICT OF INTEREST

The authors declare that there is no conflict of interests regarding the publication of this manuscript.

REFERENCES

1. Zhang S-G, Liang C-G, Zhang W-H. Recent Advances in Indazole-Containing Derivatives: Synthesis and Biological Perspectives. Molecules. 2018;23(11):2783.
2. M. Al-Ajely H. Green Synthesis of New Hydrazone Derivatives. Minar International Journal of Applied Sciences and Technology. 2022;4(3):530-535.
3. Han Mİ, GÜRol G, Yildirm T, Kalayci S, ŞAhİN F. Synthesis and antibacterial activity of hnew hydrazide-hydrazones derived from Benzocaine. Marmara Pharmaceutical Journal. 2017;21(4):961-966.
4. Salazar-Muñoz J, Zarate X, Sotomayor-Jaramillo J, Bustos C, Schott E. Synthesis and theoretical study of a new family of pyrazole derivative. J Mol Struct. 2024;1301:137267.
5. Rahim F, Ullah H, Hussain R, Taha M, Khan S, Nawaz M, et al. Thiadiazole based triazole/hydrazone derivatives: Synthesis, in vitro α-glucosidase inhibitory activity and in silico molecular docking study. J Mol Struct. 2023;1287:135619.
6. Muntadher AA-S, Shireen RR, Saba SMA-O. Synthesis and Characterization of Some New Drug Derivatives containing thiadiazole, oxadiazole, and triazole rings, and studying their antibacterial activity. Applied Chemical Engineering. 2025.
7. Khanum A, Pasha MA. Catalyst-free synthesis of new hydrazino thiazole derivatives in water under ultrasonication and evaluation of their antioxidant activity. Tetrahedron. 2024;167:134227.
8. El-Naggar AM, Zidan A, Elkaeed EB, Taghour MS, Badawi WA. Design, synthesis and docking studies of new hydrazinyl-thiazole derivatives as anticancer and antimicrobial agents. Journal of Saudi Chemical Society. 2022;26(4):101488.
9. Ahmed A, Tariq N, Abdo Ahmed W, Redwan A. synthesis and characterization of 1,2,4-traiazole derivative from methyl benzaoate with sulfur bridge links. Journal of University of Anbar for Pure Science. 2024;18(2):123-129.
10. T. Natheer R. Removal Of Mercury And Lead Metals From Their Aqueous Solution By Using New Polymers Of Triazole Derivatives. African Journal of Biomedical Research. 2024:5290-5299.
11. Mohammed AMH, Jasim SS. Synthesis, characterization and biological evaluation of quinazoline-4-one derivatives via cyclization of hydrazones. International Journal of Advanced Chemistry Research. 2024;6(2):125-133.
12. Amer H, Ali O, Salama A, gendy M, Houssin O. Synthesis of some new 1,3,4-oxadiazole derivatives bearing sugars and α-aminophosphonate derived from 4-nitrophenol as anticancer agents. National Journal of Physiology, Pharmacy and Pharmacology. 2018;2(1):1275.
13. Mukhtar S, Hassan A, Morsy N, Hafez T, Hassaneen H, Saleh F. Overview on Synthesis, Reactions, Applications, and Biological Activities of Schiff Bases. Egyptian Journal of Chemistry. 2021;0(0):0-0.
14. Damdoom WK, Al-Jeilawi OHR. Synthesis and Characterization of Some Oxazolidine and Thiazolidine Derivatives and Study of their Antioxidants Activity. Iraqi Journal of Science. 2024:6242-6252.
15. H. Abbas H, H. Abed O. Synthesis and Characterization of Some New Oxazolidinone and Thiazolidinone Derivatives Via Reaction of Schiff Bases Derived from some Amino Acids. Journal of University of Anbar for Pure Science. 2017;11(3):69-76.
16. Al-Suraify SMT, Hussien LB. Synthesis and characterization of new compounds derived from 1H-indol-5-ylamine. Applied Nanoscience. 2022;13(3):2083-2092.
17. Al-Suraify SMT, Hussien LB. Retraction Note: Synthesis and characterization of new compounds derived from 1H-indol-5-ylamine. Applied Nanoscience. 2024;14(4):719-719.
18. Synthesis of New Nitrogenous Derivatives Based On 3-Chloro–1-methyl-1H-indazole. International Journal of Pharmaceutical Research. 2020;12(sp1).
19. Synthesis and Characterization of Novel Compounds Derived From 6-methyl-2,6 dihydro[1,2,4-triazino[4,3-b] indazol-3(4H)-one. International Journal of Pharmaceutical Research. 2020;12(sp1).
20. Soliman R. Synthesis of Tetrahydrobenzothieno[2,3-d] pyrimidine and Tetrahydrobenzothieno[3,2-e[1,2,4] triazolo[4,3-c]pyrimidine Derivatives as Potential Antimicrobial Agents. Sci Pharm. 2009;77.
21. Alagöz T, Çalişkan FG, Bilgiçli HG, Zengin M, Sadeghi M, Taslimi P, et al. Synthesis, characterization, biochemical, and molecular modeling studies of carvacrol-based new thiosemicarbazide and 1,3,4-thiadiazole derivatives. Arch Pharm. 2023;356(12).
22. Kumari G, Dhillon S, Rani P, Chahal M, Aneja DK, Kinger M. Development in the Synthesis of Bioactive Thiazole-Based Heterocyclic Hybrids Utilizing Phenacyl Bromide. ACS Omega. 2024;9(17):18709-18746.
23. Kaur P, Kaur R, Goswami M. A REVIEW ON METHODS OF SYNTHESIS OF 1,2,4-TRIAZOLE DERIVATIVES. International Research Journal Of Pharmacy. 2018;9(7):1-35.
24. T Sadeek G, S Al-Ajely M, H Saleem N. Synthesis of Some Oxazine Compounds Derived from TDI and Schiff Bases. Acta Scientific Medical Sciences. 2020;4(9):120-128.

25. Abu-Hashem AA. Synthesis and antimicrobial activity of new 1,2,4-triazole, 1,3,4-oxadiazole, 1,3,4-thiadiazole, thiopyrane, thiazolidinone, and azepine derivatives. J Heterocycl Chem. 2020;58(1):74-92.
26. Patterson AL. The Scherrer Formula for X-Ray Particle Size Determination. Phys Rev. 1939;56(10):978-982.
27. Vives S, Gaffet E, Meunier C. X-ray diffraction line profile analysis of iron ball milled powders. Materials Science and Engineering: A. 2004;366(2):229-238.
28. Goldstein JI, Newbury DE, Michael JR, Ritchie NWM, Scott JHJ, Joy DC. Scanning Electron Microscopy and X-Ray Microanalysis. Springer New York; 2018. http://dx.doi.org/10.1007/978-1-4939-6676-9
29. Klessinger M. Spectrometric Identification of Organic Compounds. Von R. M. Silverstein und G. C. Bassler. John Wiley and Sons, New York-London-Sydney 1967. 2. Aufl., IX, 256 S., zahlr. Abb., geb. 75 s. Angew Chem. 1968;80(9):372-372.
30. Salem MA, Helal MH, Gouda MA, Ammar YA, El-Gaby MSA, Abbas SY. An overview on synthetic strategies to coumarins. Synth Commun. 2018;48(13):1534-1550.
31. Colthup NB, Daly LH, Wiberley SE. PREFACE. Introduction to Infrared and Raman Spectroscopy: Elsevier; 1990. p. xi-xii. http://dx.doi.org/10.1016/b978-0-08-091740-5.50003-x
32. Stojčev M. The 8051 Microcontroller, 3rd ed., I. Scott Mackenzie, Prentice Hall, Upper Saddle River, New Jersey, 1999, hardcover, 366pp., $36.95, ISBN 0-13-780008-8. Microelectron J. 1999;30(8):808-809.
33. Refaat HM, Moneer AA, Khalil OM. Synthesis and antimicrobial activity of certain novel quinoxalines. Archives of Pharmacal Research. 2004;27(11):1093-1098.
34. Ayub A, Javed T, Hamzah SK, Al-Suraify SMT, Othman MA-M, Jasim LS, et al. A review of synthesis strategies and applications of effective adsorbents for dye removal. Water Practice and Technology. 2026.
35. Eidan DM, Jasim LS, Al-Suraify SMT, Othman MA-M, Khonakdar HA. Exploring the potential of silver phosphate nanoparticles as a slow-releasing agent to develop antibacterial and biocompatible chitosan-based nanocomposite films. Int J Biol Macromol. 2025;333:148858.
36. Ma H, Wang H, Chen H, Hou H, Hu Q. Nicotine-quercetin combination alleviate ulcerative colitis via PI3K/AKT and NF-κB pathway inhibition. Chin Sci Bull. 2025;71(10):2283-2298.
37. Elizabeth B, Wanda D, Apriyanti E. The Correlation between Sleep Quality and the Prevalence of Obesity in School-Age Children. Journal of Public Health Research. 2021;10(1_suppl).
38. Suzan Sabbar M. The Association Between Iron Over Load and Tanner Stage Retardation in the Females with B-Thalassemia Major. International Journal of Research in Pharmaceutical Sciences. 2020;11(1):546-552.
39. Sabber Mutlag S. The liver injury in patients with B-thalassemia major secondary to iron over load in Thalassemia center of Diwaniyah maternity and children teaching Hospital . A clinical study in Thalassemia center of Diwaniyah maternity and children teaching Hospital. AL-QADISIYAH MEDICAL JOURNAL. 2018;13(24):39-45.
40. Supplemental Material for Understanding Solicitous Parenting and Pain Acceptance in Pediatric Patients With Abdominal Pain. Clinical Practice in Pediatric Psychology. 2022.
41. Mohsin SN, Barkat M, Ahmad A, Muddassir A, Jameel R. Frequency and Determinants of Obesity/Overweight among Undergraduate Students. Pakistan Journal of Medical and Health Sciences. 2021;15(10):2835-2837.